Physica Scripta

PAPER

Structural, elastic, and thermodynamic properties of $BaXCl_3$ (X = Li, Na) perovskites under pressure effect: *ab initio* exploration

RECEIVED
2 March 2023

REVISED
1 May 2023

ACCEPTED FOR PUBLICATION
9 May 2023

PUBLISHED
22 May 2023

Sara Chaba Mouna[1], **Missoum Radjai**[1,*], **Abdelmadjid Bouhemadou**[2], **Djamel Houatis**[1], **Djamel Allali**[3,4], **Saber Sâad Essaoud**[5] and **Saad Bin-Omran**[6]

[1] Laboratory of Physics of Experimental Techniques and Their Applications (LPTEAM), University of Medea, Algeria
[2] Laboratory for Developing New Materials and their Characterizations, University of Ferhat Abbas Setif 1, Faculty of Sciences, Department of Physics, Setif 19000, Algeria
[3] Physics and Chemistry of Materials Lab, Department of Physics, University of M'sila, 28000, M'sila, Algeria
[4] University of M'sila, Faculty of Technology, B.P. 166 Ichbilia, 28000, M'sila, Algeria
[5] Faculté des sciences, Département de physique, Laboratoire de Physique des Particules et Physique Statistique, Ecole Normale Supérieure-Kouba, BP 92, Vieux-Kouba, 16050 Algeria
[6] Department of Physics and Astronomy, College of Science, King Saud University, PO Box 2455, Riyadh 11451, Saudi Arabia
[*] Author to whom any correspondence should be addressed.

E-mail: mradjai@yahoo.com

Keywords: cubic perovskite, ab initio calculations, structural parameters, elastic constants, thermodynamic properties

Abstract

In this study, we employed the *ab initio* pseudopotential plane wave approach, utilizing the GGA-PBEsol exchange-correlation functional, to investigate the structural, elastic, and thermodynamic properties of $BaXCl_3$ (X = Li, Na) perovskites under hydrostatic pressures ranging from 0 to 18 GPa. Apart from utilizing the GGA-PBEsol functional, this study also employed the GGA-PBE, GGA-WC, and LDA functionals to simulate the exchange-correlation interactions for computing the structural parameters. Our results show that the optimized lattice parameters are in good agreement with previously predicted values. Based on the calculated elastic moduli of a single crystal, we found that both $BaLiCl_3$ and $BaNaCl_3$ perovskites retain mechanical stability under hydrostatic pressures of up to 18 GPa. Furthermore, we calculated several other important parameters that describe the polycrystalline aggregates of these compounds, including the modulus of compressibility, the shear modulus, the Poisson's ratio, Young's modulus, the speeds of sound, and the Debye temperature. Additionally, we examined the temperature and pressure dependencies of the thermal coefficients of the perovskites using the quasi-harmonic approximation. Notably, all of the results presented in this study are reported for the first time and require further confirmation through experimental investigations. We hope that our findings contribute to a more comprehensive understanding of the structural and thermodynamic properties of $BaXCl_3$ (X = Li, Na) perovskites under pressure.

1. Introduction

Perovskites, named from the Russian mineralogist Lev Alexeïevich Perovski (1792–1856), constitute a large family of solid materials resembling the mineral perovskite $CaTiO_3$ [1]. The most famous perovskite materials on Earth are fluoro-perovskites (ABF_3), oxide-perovskites (ABO_3), and nitride-perovskites (ABN_3), where *A* is usually a rare Earth, alkali metal or alkaline Earth element, and *B* is a transition metal atom [2–4]. This family of materials includes insulators, conductors, semiconductors and superconductors [3–8]. Perovskite materials possess a range of exceptional physical and chemical characteristics that have been extensively studied from both theoretical and experimental perspectives. These include exceptional structural flexibility, high light absorption, tunable bandgaps, high thermoelectric power, remarkable charge transport parameters, high mobilities of photogenerated charge carriers, spin-dependent transport, lower binding energy of exciton, ferroelectricity, and colossal magnetoresistance [7, 9–11]. These unique properties have attracted significant interest in the development of perovskite materials for a wide range of applications, including photovoltaic cells, light-emitting

diodes, sensors, lasers, and memory devices, among others [2, 7, 12–15]. In particular, the high efficiency and low cost of perovskite-based photovoltaics have spurred a significant effort towards their commercialization, with the aim of offering a viable alternative to conventional silicon-based solar cells. Furthermore, the exceptional optoelectronic properties of perovskites make them promising candidates for use in various other electronic and optical applications, such as microelectronics and telecommunications [3]. In these fields, perovskites may offer unique advantages, such as high dielectric constants and excellent optical and electrical properties. Overall, the exceptional physical and chemical properties of perovskite materials, along with their potential applications in a range of systems and devices, highlight the importance of continued research and development in this field.

Recently, ternary halide perovskites have attracted tremendous attention from materials science researchers mainly due to the impressive power conversion efficiency of their solar cells, which is attributed to their appropriate electronic and optical characteristics, such as high optical absorption, tunable bandgap, board absorption spectrum, small charge carrier effective masses, long charge diffusion lengths, and high charge carrier mobility [7–12]. Notably, the power conversion efficiency of solar cells based on halide perovskites increased from 3.8% in 2009 to 25.8% today [16–18]. Furthermore, they are cheap and easy to synthesize [16, 19–24].

Perovskite materials are renowned for their exceptional properties, which enable their excellent performance in electronic devices. However, despite the immense success of hybrid organic-inorganic halide perovskites $AM^{IV}X^{VII}3$, with A indicating a small monovalent organic molecule, M^{IV} representing a divalent group-IVA cation, and X^{VII} representing a halogen anion, in solar cell applications, they still face challenges that hinder their large-scale commercial use. The foremost issue is their poor long-term stability in devices, especially under conditions of high heat and humidity [25, 26]. Additionally, these materials are toxic due to their inclusion of the toxic element Pb [27]. Consequently, considerable efforts have been devoted to addressing the toxicity and instability concerns by seeking alternative non-toxic or low-toxicity, air-stable perovskites [27, 28]. Accordingly, researchers are actively exploring strategies for developing a more stable and less hazardous ABX_3 structure, where A, B, and X denote organic or inorganic monovalent cations, inorganic divalent cations, and halides, respectively [8]. Recently, Gomez-Peralta and Bokhimi [29] used an Artificial Neural Network to predict 134 AMX_3 (X = F, Cl, Br or I, and M = an alkali or Earth-alkali element) compounds as potential candidates to adopt the well-known perovskite structure. It was found that the predicted perovskites could find applications such as new solar cells or transparent semiconductors [8]. Among the predicted compounds, the chloro-perovskites $BaLiCl_3$ and $BaNaCl_3$ have been reported to crystalize stably in an ideal cubic structure with the $Pm\bar{3}m$ space group [29]. Note that to date, there have been no theoretical or experimental studies exploring the fundamental physical properties of these two perovskites. It is known that the mismatch between the elaborate films and the substrates can induce stresses on the films which affect their physical properties. Therefore, it is necessary to know the response of these materials to external stresses by exploring their elastic properties. Additionally, devices based on these materials are usually used at environment different from the standard conditions of temperature and pressure, so it is also necessary to determine how materials will respond to changes in their environment, especially in regards to their macroscopic physical parameters. Knowing physical and chemical properties of materials and predicting how they will respond to changes in their environment allow engineers to design better devices. Thus, the present work was devoted to the exploration of the structural, elastic, and thermodynamic properties of $BaXCl_3$ (X = Li, Na) perovskites.

2. Computational methodology and settings

The structural parameters, elastic moduli, and thermodynamic properties of the $BaXCl_3$ (X = Li, Na) crystals were investigated through the pseudopotential plane wave (PP-PW) approach [30] as implemented in the CASTEP computational software [31]. To model the exchange-correlation interactions, we utilized various functionals including GGA-PBEsol [32], GGA-PBE [33], GGA-WC [34], and LDA [35] for geometry optimization. However, for other properties considered, we used only the GGA-PBEsol functional. Interactions of the valence states: Ba: $5s^25p^66s^2$, Li: $1s^22s^1$, Cl: $3s^23p^5$ and Na: $2s^22p^63s^1$ with core ions were treated via OTFG ultrasoft pseudopotentials [36]. A plane wave basis set with a cutoff energy of 650 eV was used to develop the electron wave functions. Integration over the reciprocal space was replaced by a summation on special points in the Brillouin zone (BZ) defined via a sampling of BZ to a 12 × 12 × 12 Monkhorst-Pack grid [37]. Relaxations of the structural parameters to their equilibrium state were accomplished through the BFGS approach [38]. Calculations were performed with total energy convergence, maximum force tolerance, maximum stress and maximum displacement less than 5.0×10^{-6} eV/atom, 0.01 eV/ Å, 0.02 GPa and 5.0×10^{-4} Å, respectively. Numerical estimates of the elastic constants were obtained via the stress-strain approach as included in the CASTEP code [30]. The variations of some macroscopic physical parameters with temperature and pressure were explored through the quasi-harmonic approximation as incorporated in the GIBBS calculation software [39].

Table 1. Optimized lattice parameter (a, in Å), modulus of compressibility (B, in GPa), its pressure derivative (B', dimensionless), tolerance factor (t), Octahedral factor (μ), the formation enthalpy (ΔH, in eV/atom) and the cohesive energy (E_{coh}, in eV/atom) for BaXCl$_3$ (X = Li, Na) compounds.

	$BaLiCL_3$		$BaNaCl_3$	
	Present work	Other [25]	Present work	Other [25]
α	4.7994[a]	4.8165	5.0463 [a]	5.0805
	4.9051[b]		5.1549 [b]	
	4.7985[c]		5.0472 [c]	
	4.7180[d]		4.9479 [d]	
B	38.6[e], 38.6[f]		32.0[e], 31.9[f]	
	39.3[g]		32.7[g]	
B'	4.63[e], 4.62[f]		4.71[e], 4.71[f]	
	4.60[g]		4.79[g]	
t	0.87		0.79	
μ	0.42		0.56	
ΔH	−3.6535		−3.4677	
E_{coh}	−4.2489		−4.0181	

[a] obtained using GGA-PBEsol
[b] obtained using GGA-PBE
[c] obtained using GGA-PBE
[d] obtained using GGA-PBE
[e] Obtained from Birch E-V EOS;
[f] Obtained from Birch-Murnaghan P−V EOS
[g] Obtained from Vinet P−V EOS.

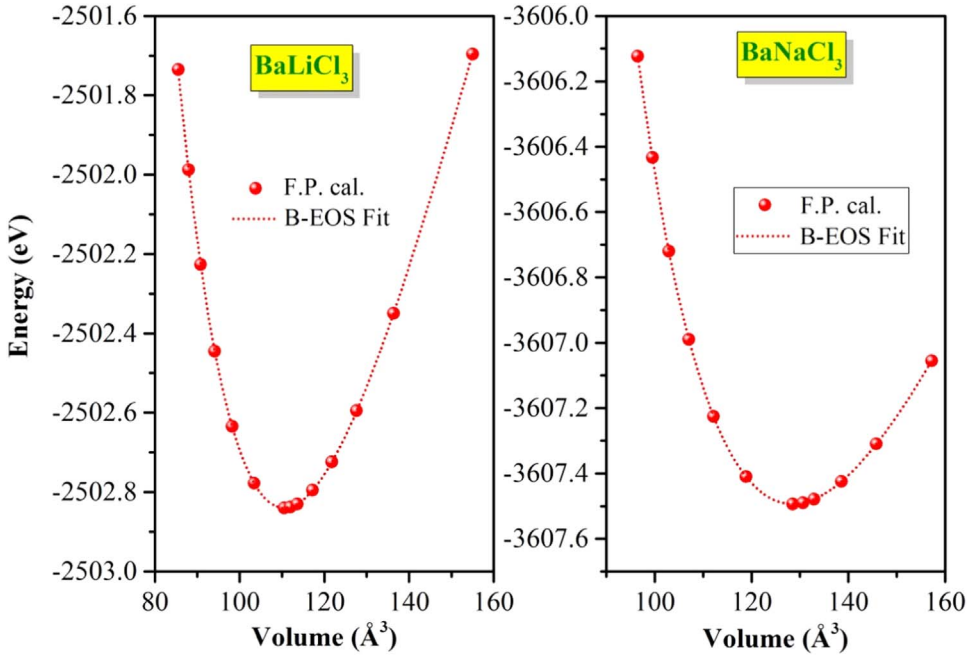

Figure 1. Variation of total energy with unit cell volume (E-V) for $BaLiCL_3$ and $BaNaCl_3$. The symbols display the E-V data obtained via first-principles calculations (F.P. cal.) and the dashed line displays the fit of the E-V data to the Birch equation of state (B-EOS).

3. Results and discussion

3.1. Structural parameters

The chloro-perovskites BaXCl$_3$ (X = Li, Na) crystalize in a cubic crystal system with the space group $Pm\bar{3}m$ (#221) [29]. The Ba atom takes position at the corners of the cube (0, 0, 0), the X atom is located at the center of the cube (0.5, 0.5, 0.5), and the Cl atoms are positioned at the face centers of the cube (0.5, 0, 5, 0), (0.5, 0, 0.5), (0, 0.5, 0.5). The geometry has been optimized using the GGA-PBEsol, GGA-PBE, GGA-WC and LDA functionals. The optimized lattice parameters (a) for $BaLiCl_3$ and $BaNaCl_3$ are given in table 1. It is worth noting that the

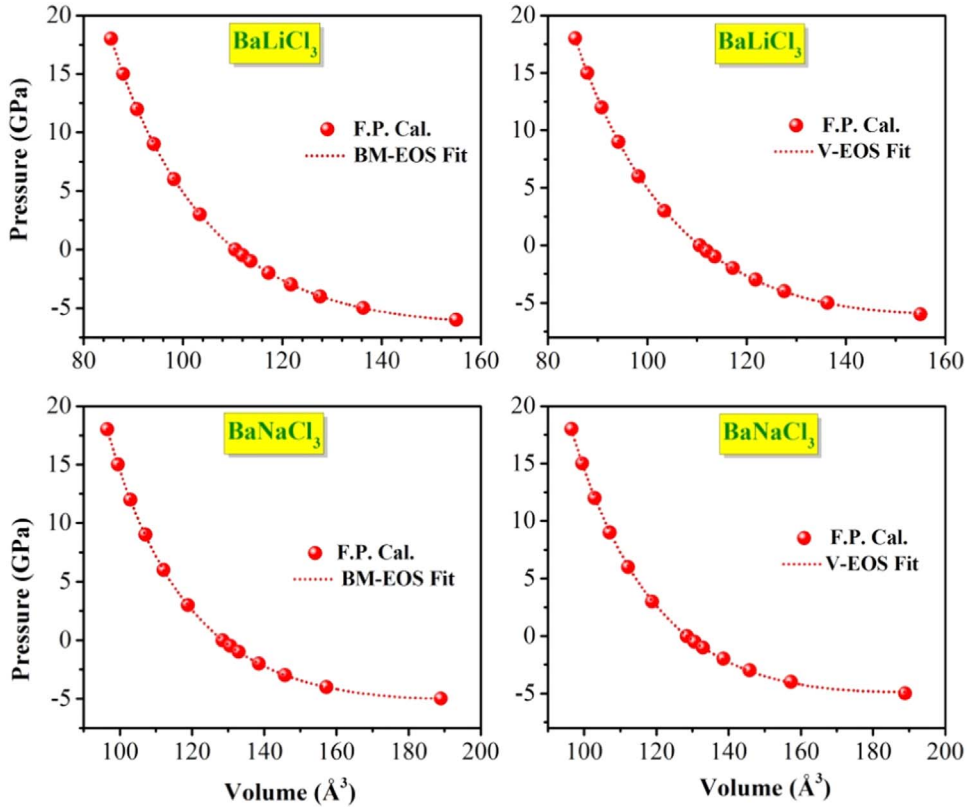

Figure 2. Variation of unit cell volume with pressure (*P-V*) for $BaLiCL_3$ and $BaNaCl_3$. The symbols display the *P-V* data obtained via first-principles calculations (F.P. cal.) and the dashed lines display the fits of the *P-V* data to the Birch-Murnaghan equation of state (BM-EOS) and the Vinet equation of state (V-EOS).

variation between the values obtained using different versions of the GGA functional is minimal, with a difference of less than 0.35% (0.67%) observed for $BaLiCl_3$ ($BaNaCl_3$). However, when using the LDA functional, the results obtained were approximately 2% lower compared to those obtained using the GGA functionals. We appreciate that our results are consistent with those previously reported in the literature [29].

The values of the modulus of compressibility (*B*) and its pressure derivative (*B*') for $BaLiCl_3$ and $BaNaCl_3$ were estimated by fitting the variation of total energy (*E*) with unit cell volume (*V*) to the Birch equation of state (EOS) [40] and the variation of unit cell volume (*V*) with hydrostatic pressure (*P*) to the Birch-Murnaghan and Vinet equations of state [41, 42], as shown in figures 1 and 2. The values of *B* and *B*' are tabulated in table 1. One appreciates the concordance of the values of *B* obtained using the adjustment by different equations of state, proving the reliability of the results obtained. The moderate values of *B* for the two compounds under consideration highlight the weak resistance of these materials to compression.

We calculated the Goldsmith tolerance factor (*t*) and octahedral factor (μ) to assess the structural stability of the perovskite compounds being considered using the following relationships [43, 44]:

$$t = \frac{r_A + r_X}{\sqrt{2}\,(r_B + r_X)}, \quad \mu = \frac{r_B}{r_X}$$

In this context, r_A, r_B, and r_X refer to the ionic radii of the A, B, and X ions in the ABX_3 perovskite. The perovskite structure is considered stable if the values of '*t*' are between 0.7 and 1.0 [44]. For the $BaXCl_3$ compounds where X is either Li or Na, the calculated values of the Goldsmith tolerance factor and octahedral factor (see table 1) fell within the aforementioned range, indicating the structural stability of these compounds in their cubic structure. In order to gain a better understanding of the structural and thermodynamic stabilities of the $BaXCl_3$ (X = Li, Na) perovskites, we have calculated their formation enthalpy (ΔH) and cohesive energy (E_{coh}) using the following expressions [45]:

$$\Delta H = \frac{1}{n_{Ba} + n_X + n_{Cl}} \times [E_{tot}^{BaXCl_3} - (n_{Ba}E_{tot}^{Ba(solid)} + n_X E_{tot}^{X(solid)} + n_{Cl}E_{tot}^{Cl(solid)})]$$

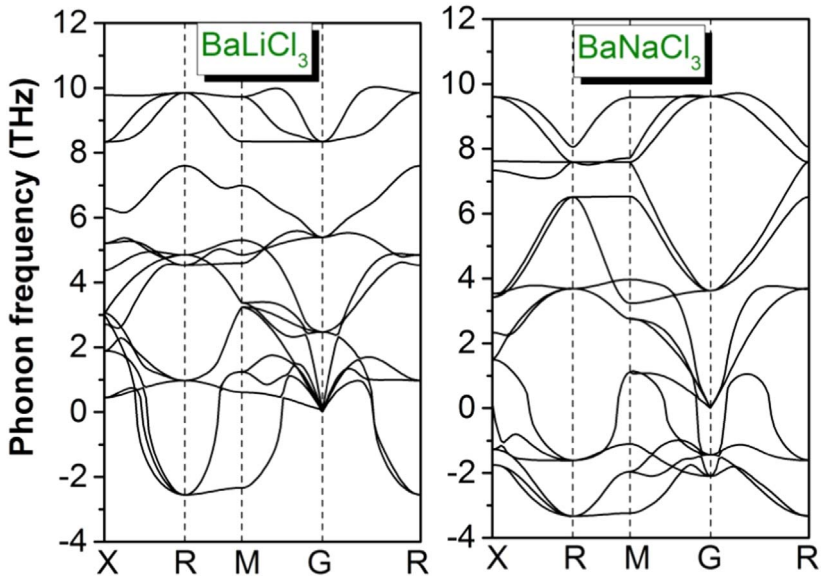

Figure 3. Phonon dispersion curves for the $BaLiCl_3$ and $BaNaCl_3$ compounds.

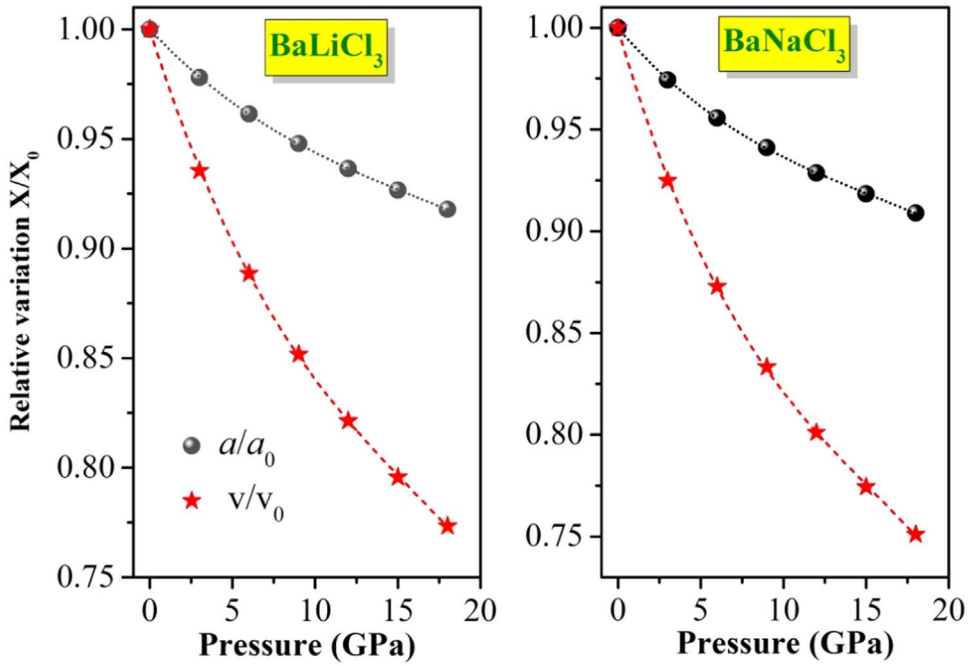

Figure 4. Pressure dependence of a/a_0 and V/V_0 for $BaLiCL_3$ and $BaNaCl_3$. a and V are the lattice parameter and unit cell volume, respectively, at a pressure P and a_0 and V_0 their corresponding values, respectively, at zero pressure.

$$E_{coh} = \frac{1}{n_{Ba} + n_X + n_{Cl}} \times [E_{tot}^{BaXCl_3} - (n_{Ba}E_{tot}^{Ba(atom)} + n_X E_{tot}^{X(atom)} + n_{Cl}E_{tot}^{Cl(atom)})]$$

In this context, the total energy of the primitive cell of $BaXCl_3$ is represented by $E_{tot}^{BaXCl_3}$, while the total energies per atom of the solid state of the pure Ba, X (X = Li, Na) and Cl elements are represented by $E_{tot}^{Ba(solid)}$, $E_{tot}^{X(solid)}$ and $E_{tot}^{Cl(solid)}$, respectively. $E_{tot}^{Ba(atom)}$, $E_{tot}^{X(atom)}$ and $E_{tot}^{Cl(atom)}$ represent the total energies of the isolated Ba, X, and Cl atoms, while n_{Ba}, n_X and n_{Cl} represent the number of Ba, X, and Cl atoms in the primitive cell. The calculated values for the formation enthalpies and cohesive energies of $BaXCl_3$ (X = Li, Na) are shown in table 1. Notably, both compounds have negative formation enthalpies and cohesive energies, indicating their structural and energetic stabilities in the cubic structure.

Table 2. Predicted monocrystalline elastic constants (C_{ij}, in GPa) for BaXCl$_3$ (X = Li, Na) compounds.

Compound	C_{11}	C_{12}	C_{44}
$BaLiCl_3$	72.5	21.5	22.1
$BaNaCl_3$	75.3	10.3	8.6

In order to evaluate the dynamic stability of the compounds under investigation, we utilized the linear response method within the density functional perturbation theory (DFPT) as implemented in the CASTEP code [30] to compute their phonon dispersion diagrams. The resulting phonon dispersion curve is displayed in figure 3. It is widely accepted that a phonon dispersion curve lacking soft modes (imaginary modes; negative frequencies) indicates dynamic stability in the corresponding material [46]. Conversely, the presence of soft modes (negative frequencies) in the phonon dispersion spectra for the material in question (as depicted in figure 3) implies dynamic instability in certain vibrational modes. Soft modes have been known to trigger lattice instability, which may result in a structural phase transition. Additionally, the presence of soft modes at all points in the Brillouin zone may suggest that the probability of successfully synthesizing the compound under normal conditions is low. It should be noted that the occurrence of negative frequencies in the phonon dispersion curve of materials is not necessarily an indication that these materials, in their crystal structure, are unstable in the majority of cases. In fact, a variety of synthesized materials have exhibited vibrational soft modes [47–49].

Figure 4 illustrates variations of a/a_0 and V/V_0 with pressure; a and V are the lattice parameter and unit cell volume, respectively, at a pressure P, and a_0 and V_0 are their corresponding values at zero pressure). Evolutions of a/a_0 and V/V_0 with P fit well to third-order polynomials.

$$BaLiCl_3\begin{cases}\dfrac{a}{a_0} = 1 - 8.48\times10^{-3}p + 3.61\times10^{-4}p^2 - 8.09\times10^{-6}P^3\\ \dfrac{V}{V_0} = 1 - 2.54\times10^{-2}p + 1.2\times10^{-3}p^2 - 2.76\times10^{-5}P^3\end{cases}$$

$$BaNaCl_3\begin{cases}\dfrac{a}{a_0} = 1 - 1.03\times10^{-2}p + 5.09\times10^{-4}p^2 - 1.23\times10^{-5}P^3\\ \dfrac{V}{V_0} = 1 - 3.09\times10^{-2}p + 1.68\times10^{-3}p^2 - 4.15\times10^{-5}P^3\end{cases}$$

The calculated linear and volume compressibilities (β_a and β_V), which are 8.48×10^{-3} and 2.54×10^{-2}, respectively, for $BaLiCl_3$, and 1.03×10^{-2}, and 3.09×10^{-2}, respectively, for $BaNaCl_3$, were used to evaluate the modulus of compressibility (B) using the following relationships [45, 50]: $B = \dfrac{1}{3\,\beta_a}$; $B = \dfrac{1}{\beta_V}$. The obtained B values using the aforementioned relationships are: 39.3, and 39.4 GPa for $BaNaCl_3$, and 32.4 and 32.4 GPa for $BaLiCl_3$. These results are consistent with the corresponding values derived from the E–V and P–V fits with the corresponding equations of state; see table 1.

3.2. Elastic properties

3.2.1. Monocrystalline elastic constants

Monocrystalline elastic constants (C_{ij}) are key physical parameters for describing the mechanical properties of materials. C_{ij} provide information on how a crystal deforms under external stress and then returns to its original shape once the stress is removed [51]. Many physical properties of the crystal, such as its mechanical stability, elastic anisotropy, Debye temperature, and elastic wave propagation velocity, can be predicted from its C_{ij}. Numerical estimates of the independent monocrystalline elastic constants, namely C_{11}, C_{12}, and C_{44}, of the cubic perovskites $BaLiCl_3$ and $BaNaCl_3$ at zero pressure are given in table 2. Note the unavailability of data concerning the C_{ij} values in the literature for the considered materials; thus, these reported data are the first theoretical prediction of these physical parameters. The predicted C_{ij} values for both materials under consideration satisfy the required conditions for the mechanical stability of a cubic system [52, 53], viz. $(C_{11} - C_{12}) > 0$; $(C_{11} + 2C_{12}) > 0$; $C_{11} > 0$; $C_{44} > 0$; $C_{12} < B < C_{11}$. This highlights the mechanical stability of $BaLiCl_3$ and $BaNaCl_3$ at zero pressure. One notes the moderate values of C_{ij}, which indicate the weak resistance of these materials to external stresses. The value of C_{11}, which characterizes the resistance to compression/elongation along the a-axis, is larger than the values of C_{12} and C_{44}, which characterize the resistance to shear, suggesting that these materials are more resistant to compression/elongation than to shear.

Figure 5 shows C_{ij} evolutions with hydrostatic pressure from 0 to 18 GPa. The calculated C_{ij} values at the pressures: 0, 3; 6, 9, 12, 15 and 18 GPa verify the required conditions of the mechanical stability under pressure

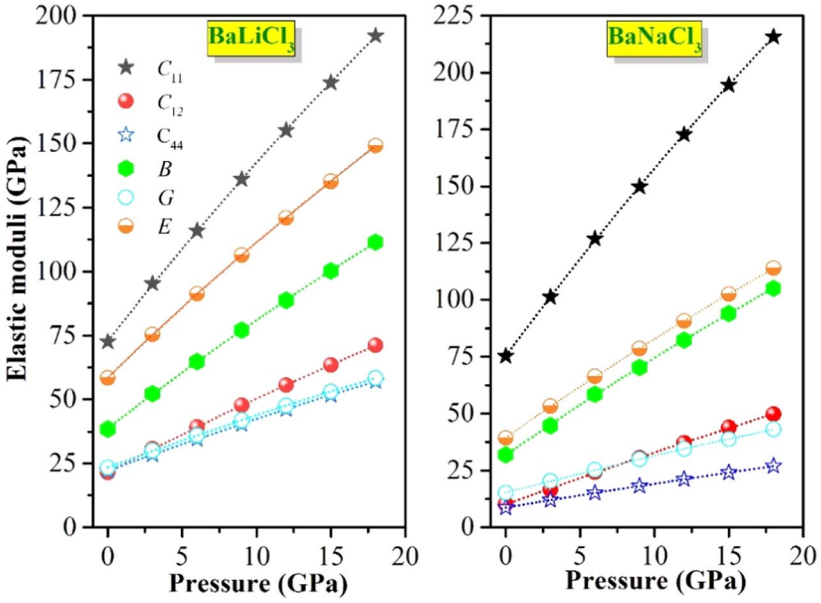

Figure 5. Evolutions of the elastic moduli: C_{11}, C_{12}, C_{44}, B, G, and E with pressure for $BaLiCl_3$ and $BaNaCl_3$ compounds.

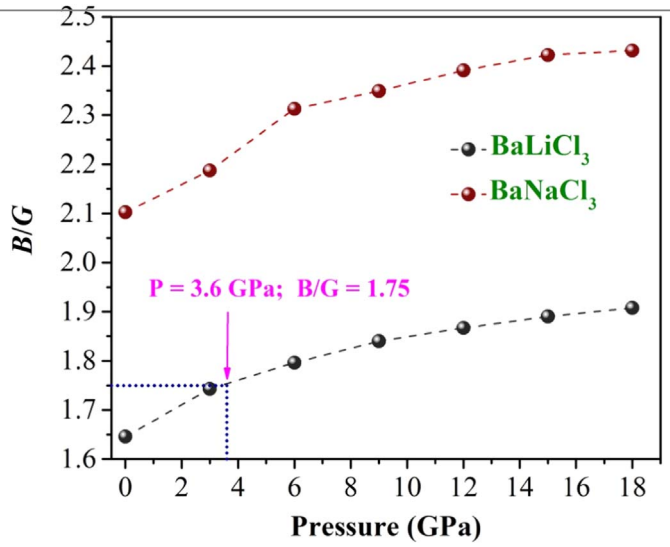

Figure 6. Variation of the B/G ratio versus pressure for $BaLiCl_3$ and $BaNaCl_3$.

Table 3. Predicted isotropic modulus of compressibility (B, in GPa), modulus of shear (G, in GPa), Young's modulus (E, in GPa), Poisson's ratio (σ), Debye temperature (θ_D, K), and transverse, longitudinal, and average sound velocities (V_t, V_l, and V_m, in m s^{-1}) for $BaLiCl_3$ and $BaNaCl_3$ materials. G_V and G_R are the G values calculated using the Voigt and Reuss approximations, respectively.

Compound	B	G_V	G_R	G	B/G	E	σ	V_l	V_t	V_m	θ_D
$BaLiCl_3$	38.5	23.44	23.32	23.4	1.64	58.3	0.247	2492.3	4301.7	2766.0	293.3
$BaNaCl_3$	31.9	18.16	12.20	15.2	2.10	39.3	0.294	2099.2	3890,9	2343.2	236.3

effect [54]: $(C_{11} - P) > |C_{12} + P|$; $(C_{11} - P) > 0$, $(C_{44} - P) > 0$, $(C_{11} + 2C_{12} + P) > 0$. These suggest that $BaXCl_3$ (X = Li, Na) compounds are still mechanically stable even under pressure. Figure 4 shows that C_{ij} increase almost linearly with increasing pressure. C_{44} is the least pressure sensitive while C_{11} is the most pressure sensitive. The variations of C_{ij} as a function of the pressure adjust well by the following polynomials of the second order:

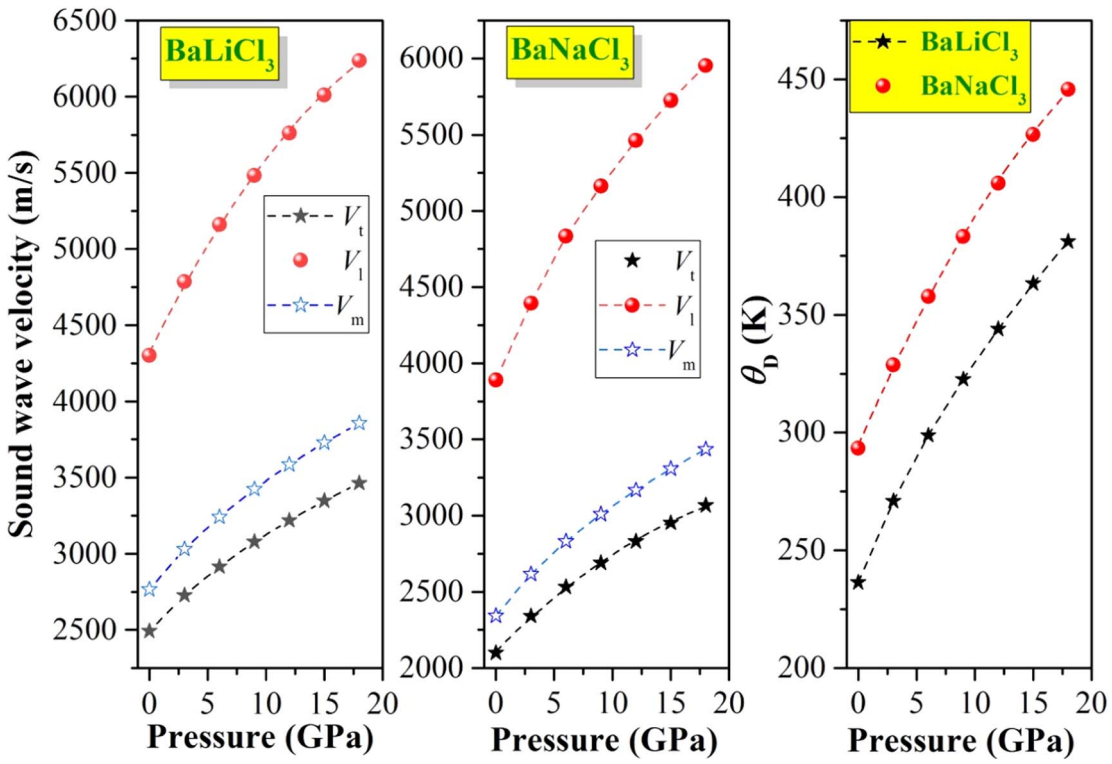

Figure 7. Variations of Debye temperature (θ_D) and of isotropic longitudinal, transversal, and mean sound velocities (V_l, V_t, and V_m) with pressure for $BaLiCl_3$ and $BaNaCl_3$.

$$BaLiCl_3\begin{cases} C_{11} = 72.85 + 7.42P - 4.56 \times 10^{-2}P^2 \\ C_{12} = 21.58 + 3.02P - 1.51 \times 10^{-2}P^2 \\ C_{44} = 22.12 + 2.12P - 1,\ 03 \times 10^{-2}P^2 \end{cases}$$

$$BaNaCl_3\begin{cases} C_{11} = 75.37 + 8.81P - 5.74 \times 10^{-2}P^2 \\ C_{12} = 9.98 + 2.39P - 9.94 \times 10^{-3}P^2 \\ C_{44} = 8.65 + 1.09P - 4.31 \times 10^{-3}P^2 \end{cases}$$

3.2.2. Polycrystalline elastic parameters

Generally, a pair of isotropic elastic parameters, namely the isotropic modulus of compressibility (B) and isotropic shear modulus (G), is used to characterize the elastic characteristics of the polycrystalline aggregate phase of a material. Theoretically, B and G of the polycrystalline aggregate phase of a material can be estimated numerically from the elastic constants (C_{ij}) of its monocrystalline phase through the Voigt-Reuss-Hill (VRH) approaches [54–58]. Another pair of isotropic elastic moduli usually used to characterize mechanical properties of the polycrystalline aggregates of a material, namely the Young's modulus (E) and Poisson's coefficient (σ), can be also estimated numerically from the B and G values using well-known relationships [59]. Numerical estimates of the isotropic elastic parameters B, G, E and σ for the polycrystalline phases of $BaLiCl_3$ and $BaNaCl_3$ are provided in table 3. Pressure dependencies of B, G, and E are represented in figure 5. Variations of B, G and E as a function of pressure fit well with second-order polynomials:

$$BaLiCl_3\begin{cases} B = 38.,67 + 4.49P - 2.53 \times 10^{-2}P^2 \\ G = 2347 + 215P - 123 \times 10^{-2}P^2 \\ E = 58.57 + 5.60P - 3.25 \times 10^{-2}P^2 \end{cases}$$

$$BaNaCl_3\begin{cases} B = 31.77 + 2.15P - 2.57 \times 10^{-2}P^2 \\ G = 15.26 + 1.71P - 9.55 \times 10^{-2}\ P^2 \\ E = 39.49 + 4.59P - 2.59 \times 10^{-2}\ P^2 \end{cases}$$

From the results obtained, it can be noted:

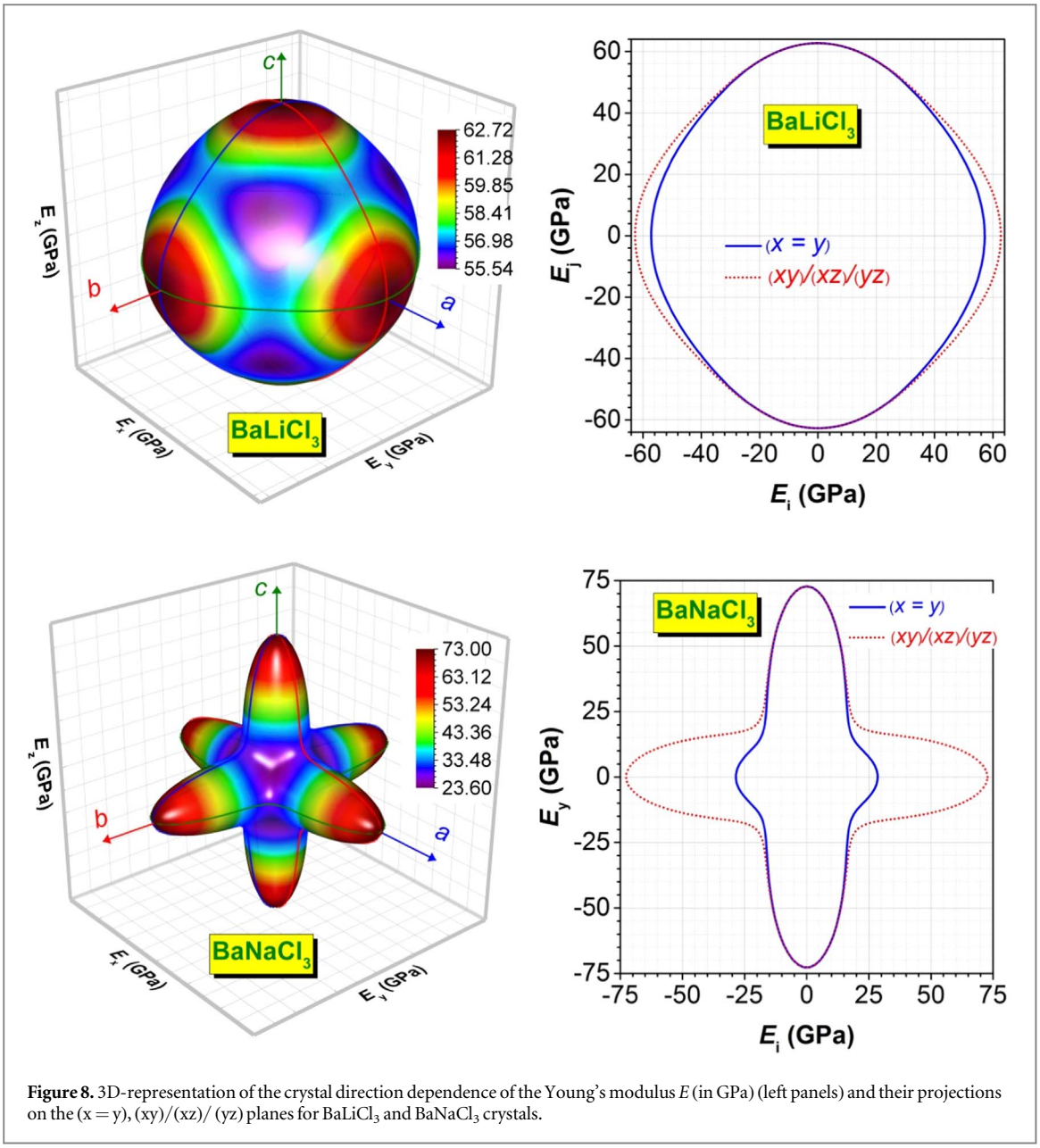

Figure 8. 3D-representation of the crystal direction dependence of the Young's modulus *E* (in GPa) (left panels) and their projections on the (x = y), (xy)/(xz)/ (yz) planes for $BaLiCl_3$ and $BaNaCl_3$ crystals.

(i) The values of the elastic parameters *B*, *G* and *E* are moderate, highlighting the weak resistance of the title materials to applied deformations.

(ii) The B value deduced from the Cij values is in good agreement with the corresponding value deduced from the adjustment of the E-V and P-V data with equations of state, confirming the reliability of the performed calculations.

An empirical criterion proposed by Pugh [60] is widely used to distinguish ductile from brittle materials. A material is ductile (brittle) when the B/G ratio is greater than 1.75 (less than 1.75). Figure 6 shows that B/G for $BaLiCl_3$ is less than 1.75 when the applied hydrostatic pressure is in the range of 0–3.6 GPa, suggesting that $BaLiCl_3$ is brittle if it is under pressure in the aforementioned range, and ductile if the applied pressure is in the range of 3.6–18 GPa. For $BaNaCl_3$, B/G is always greater than 1.75 for applied hydrostatic pressure in the range of 0–18 GPa, suggesting that it is ductile in nature even under pressure in this range. The variation in the B/G ratio observed between BaLiCl3 and $BaNaCl_3$ is primarily attributed to the disparity in ionic radius (R) between the Na and Li atoms. Specifically, the R value of Na is greater than that of Li.

(iii) The stability of a crystal against shear deformation can be characterized by the Poisson's ratio (σ). The extreme values of σ are -1 and 0.5, where the lower limit corresponds to the case when the material does not change its shape and to the upper limit when the volume does not change [61, 62]. The Poisson's ratio, a fundamental mechanical property, is widely used to distinguish ductile and brittle materials. Specifically, ductile materials are characterized by Poisson's ratios larger than 0.26, while brittle materials exhibit

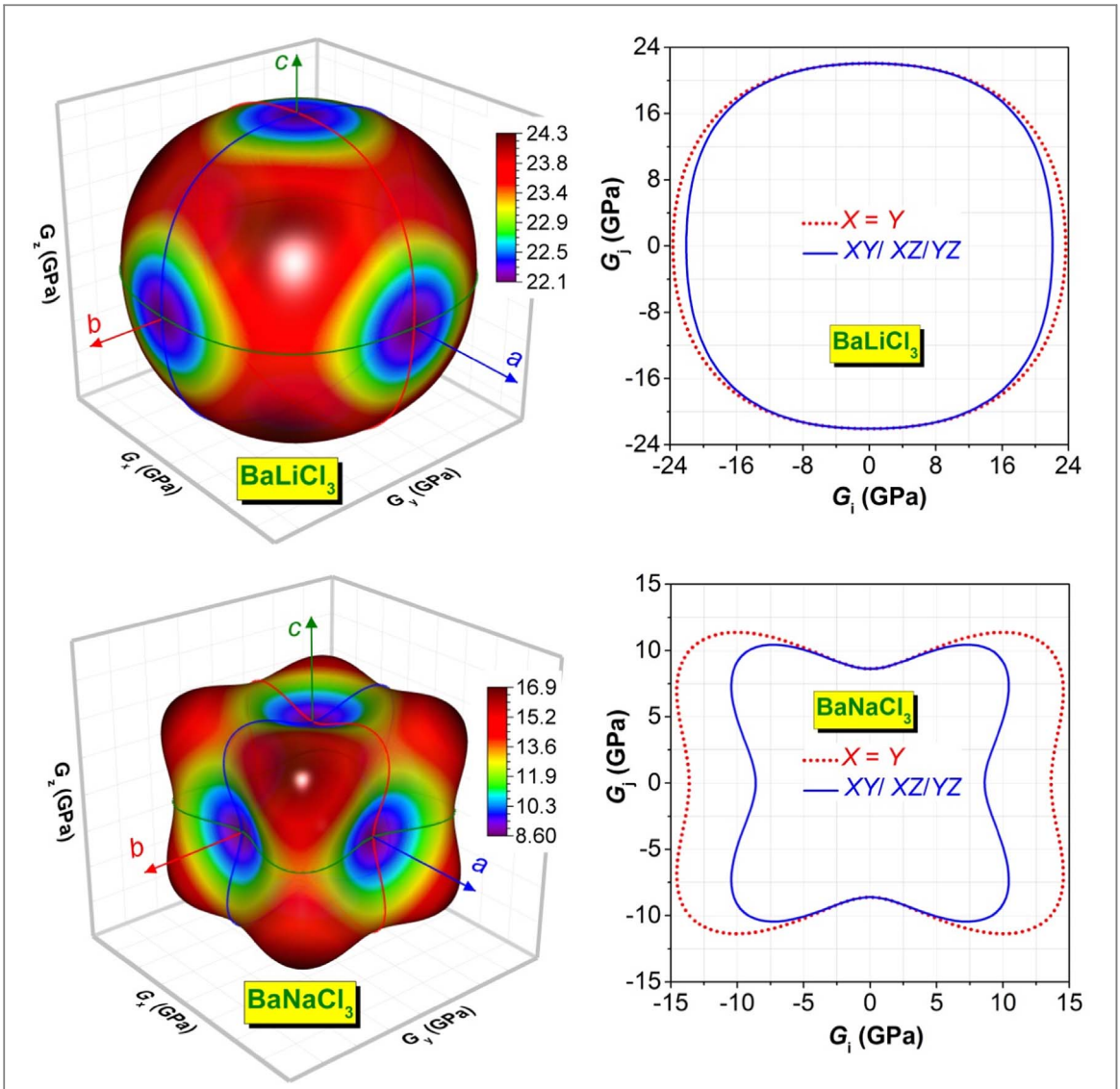

Figure 9. 3D-representation of the crystal direction dependence of the shear modulus *G* (in GPa) (left panels) and their projections on the (x = y) and (xy)/(xz)/(yz) planes for $BaLiCl_3$ and $BaNaCl_3$ crystals.

Poisson's ratios smaller than 0.26 [63]. Our experimental findings indicate that BaLiCl3 ($\sigma = 0.24$) is a brittle material, whereas BaNaCl3 ($\sigma = 0.29$) is ductile. This conclusion corroborates the outcomes derived from Pugh's ratio, a widely accepted criterion for the ductility and brittleness of materials. The obtained values for σ show that a large volume change is associated with the shear deformation of the considered materials.

(iv) The Debye temperature (θD), and the isotropic longitudinal, transversal and mean elastic wave velocities (Vl, Vt and Vm) are fundamental physical parameters that relate elastic and thermodynamic properties of solid materials, such as melting temperature, specific heat and vibrational entropy. These important physical parameters can be deduced from the isotropic elastic moduli B and G [64–69]. Debye temperature can be calculated from the value of the average elastic wave velocity (Vm) by this relationship [70, 71]:

$$\theta_D = \frac{h}{k_B}\left(\frac{3n}{4\pi} \times \frac{\rho N_A}{M}\right)^{\frac{1}{3}} \times V_m$$

In this context, V_m

$$= \left(\frac{1}{3}\left(\frac{2}{V_t^3} + \frac{1}{V_l^3}\right)\right)^{-\frac{1}{3}},\ V_l = \left(\frac{3B + 4G}{3\rho}\right)^{\frac{1}{2}},\ V_t = \left(\frac{G}{\rho}\right)^{\frac{1}{2}}$$

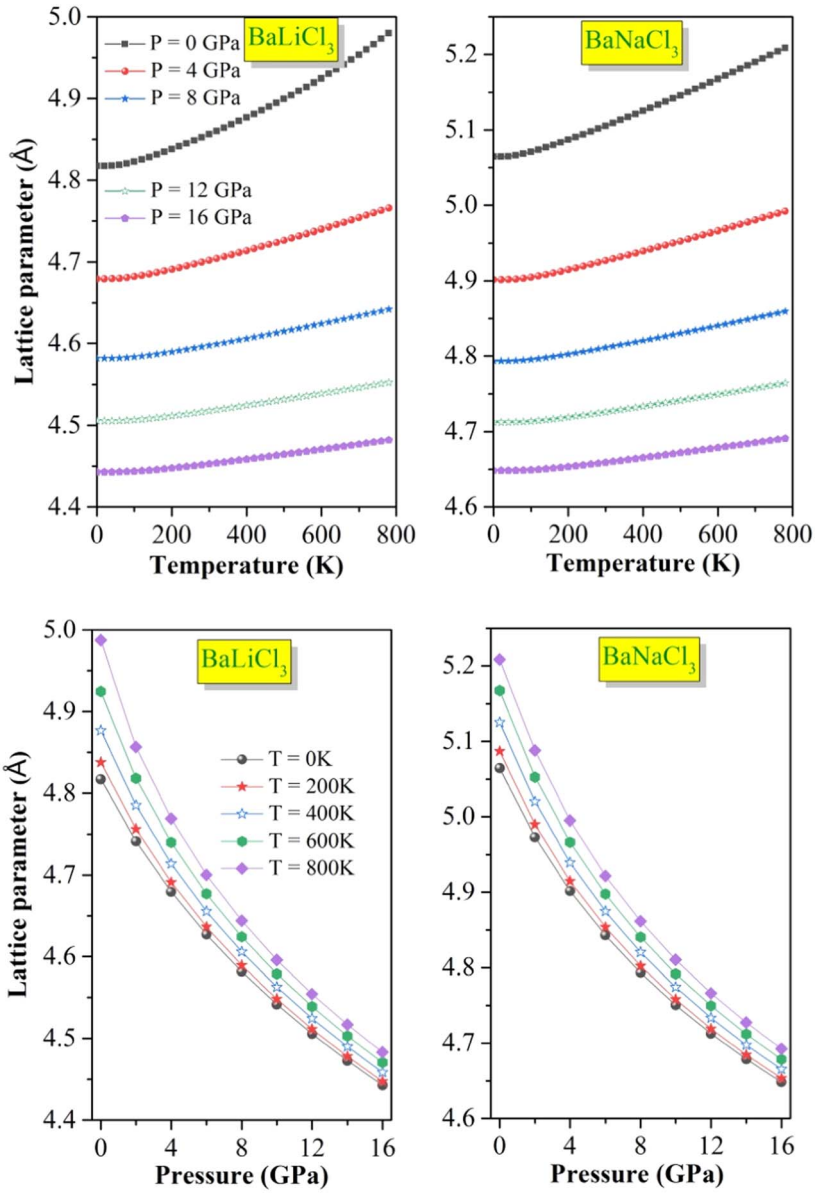

Figure 10. Evolutions of lattice parameter (*a*) with temperature at fixed pressures and with pressure at fixed temperature for of $BaLiCl_3$ and $BaNaCl_3$ compounds.

Here, ρ is the mass density, h and k_B are the Planck and Boltzmann constants, respectively, N_A is the Avogadro number, M is the molecular weight, n is the number of atoms per unit cell and V_l, V_t ,V_m are the longitudinal, transverse and average wave velocities, respectively. Predicted numerical estimates for θ_D, V_l, V_t, and V_m for $BaLiCl_3$ and $BaNaCl_3$ are given in table 3. The Debye temperature represents the temperature at which the atomic vibrations in the lattice become large enough to weaken the interatomic bonds and reduce the stiffness of the material. Therefore, materials with higher Debye temperatures tend to be stiffer, as they require higher temperatures to disrupt the interatomic bonding forces and reduce their stiffness. Conversely, materials with lower Debye temperatures tend to be softer and more deformable, as they experience weaker interatomic bonding forces that are easier to disrupt. The calculated elastic moduli values indicate that $BaLiCl_3$ is relatively stronger than $BaNaCl_3$. This difference in strength between the two materials can explain why the Debye temperature of $BaLiCl_3$ is somewhat higher than that of $BaNaCl_3$. In general, materials with higher strength have stronger interatomic bonds, which require higher temperatures to break down the lattice structure and reduce the stiffness of the material. Therefore, the somewhat higher strength of $BaLiCl_3$ can lead to a somewhat higher Debye temperature compared to $BaNaCl_3$, which is consistent with the observed trend.

Figure 7 shows the variations of the values of θ_D, V_t, V_l, and V_m of $BaLiCL_3$ and $BaNaCl_3$ with pressure in a range of 0 to 18 GPa. One notes that the aforementioned parameters increase with increasing pressure. The θ_D, V_l, V_t, and V_m values of $BaLiCl_3$ are larger than those of $BaNaCl_3$. The average sound velocity and Debye

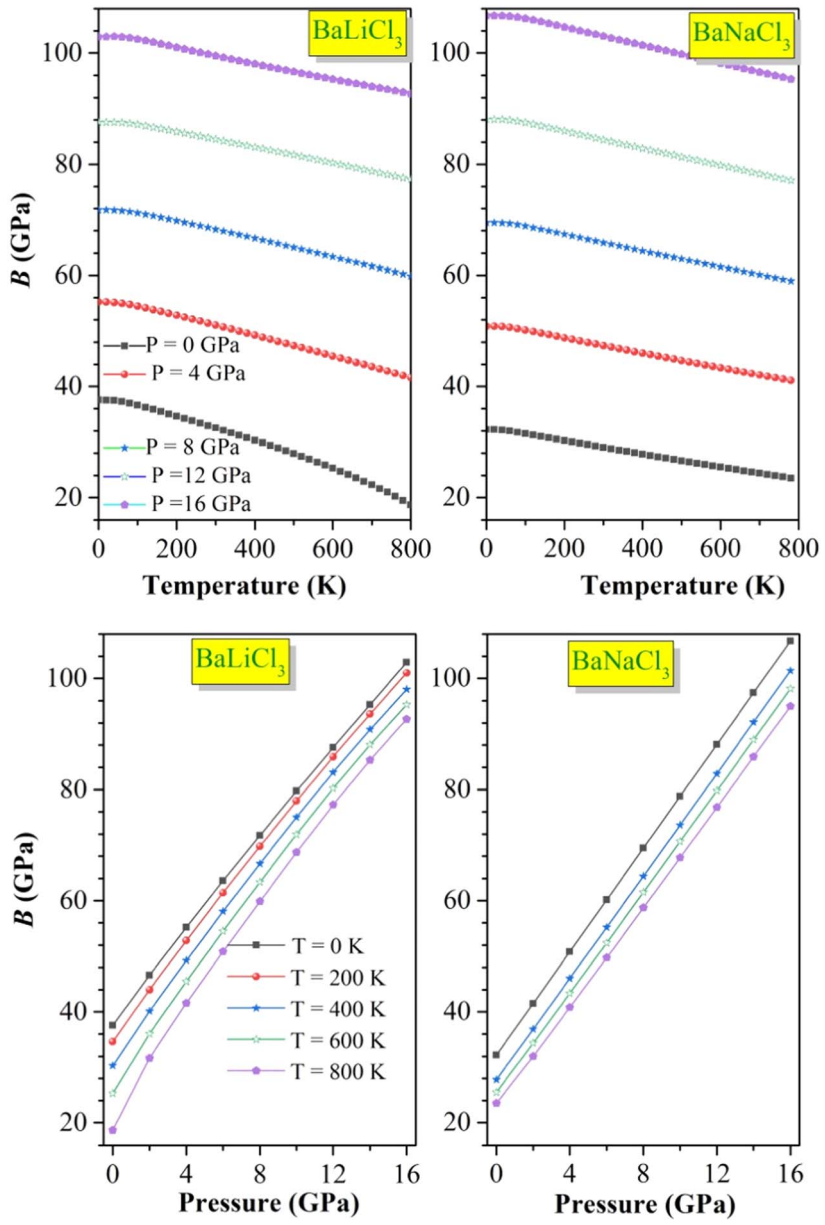

Figure 11. Evolutions of the modulus of compressibility (*B*) with temperature at fixed pressures and with pressure at fixed temperatures for $BaLiCl_3$ and $BaNaCl_3$ perovskites.

temperature are both closely related to the interatomic bonding forces and vibrational motion of atoms in the crystal lattice. There is a relationship between the average sound velocity (*V*m) and the Debye temperature (θ_D) of materials, as it is shown by the aforementioned relationship. The average sound velocity represents the speed of sound waves propagating through the material, which is related to the stiffness and interatomic bonding forces in the crystal lattice. On the other hand, the Debye temperature is related to the thermal vibrations of atoms in the crystal lattice, which can influence the interatomic bonding forces and stiffness of the material. In general, materials with higher average sound velocities tend to have higher Debye temperatures, as the higher stiffness and stronger interatomic bonding forces in the lattice require higher temperatures to break down the lattice structure and reduce the stiffness of the material. Conversely, materials with lower average sound velocities tend to have lower Debye temperatures, as the weaker interatomic bonding forces and lower stiffness make the lattice structure easier to disrupt. Therefore, the relationship between V_m and θ_D can be used to predict the thermal and mechanical properties of materials, as the average sound velocity and Debye temperature are both closely related to the interatomic bonding forces and vibrational motion of atoms in the crystal lattice. As pressure intensifies, the interatomic bonding forces within the crystal lattice also intensify. This phenomenon accounts for the rise in both Debye temperature and average sound velocity as pressure increases. The variations of the Debye temperature and sound velocities with pressure are well adjusted second-order polynomials:

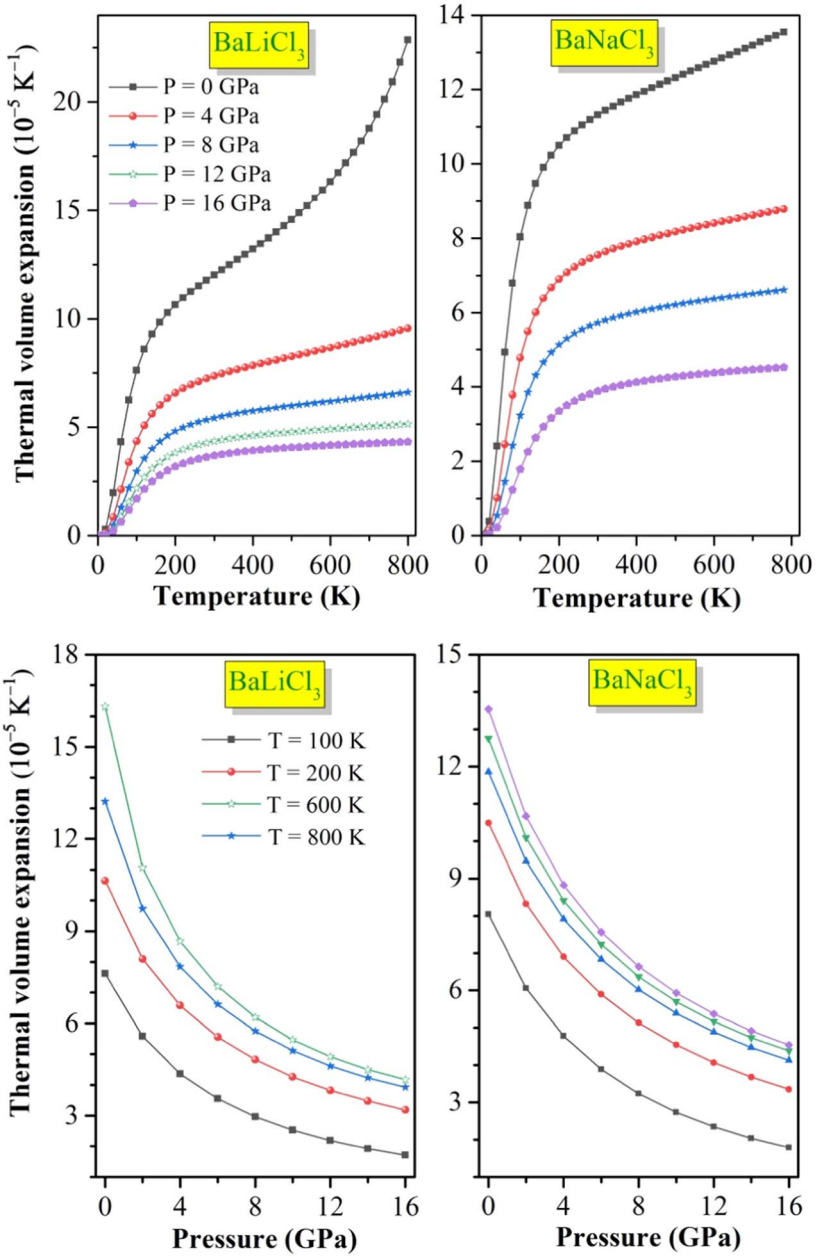

Figure 12. Evolutions of the thermal volume expansion coefficient (α)with temperature at fixed pressures and with pressure at fixed temperatures for $BaLiCl_3$ and $BaNaCl_3$ perovskites.

$$\mathrm{BaLiCl_3}\begin{cases} V_t = 2501.45 + 75.53P - 1.24P^2 \\ V_l = 4322.59 + 153.24P - 2.65P^2 \\ V_m = 2776.54 + 85.08P - 1.41P^2 \\ \theta_D = 294.54 + 11.41P - 0.17P^2 \end{cases}$$

$$\mathrm{BaNaCl_3}\begin{cases} V_t = 2110.33 + 76.87P - 1.34P^2 \\ V_l = 3906.97 + 168.18P - 3.07P^2 \\ V_m = 2355.46 + 86.87P - 1.52P^2 \\ \theta_D = 237.69 + 11.05P - 0.17P^2 \end{cases}$$

3.2.3. Elastic anisotropy

The elastic anisotropy of crystals is a key important parameter that needs to be evaluated as it has implications in engineering science. Indeed, mechanical failures and microcracks easily occur in crystals with strong elastic anisotropy [47, 72]. Therefore, it is of great importance to estimate the degree of elastic anisotropy of crystals in order to hopefully find procedures that will improve the crystal's resistance to microcracking and mechanical

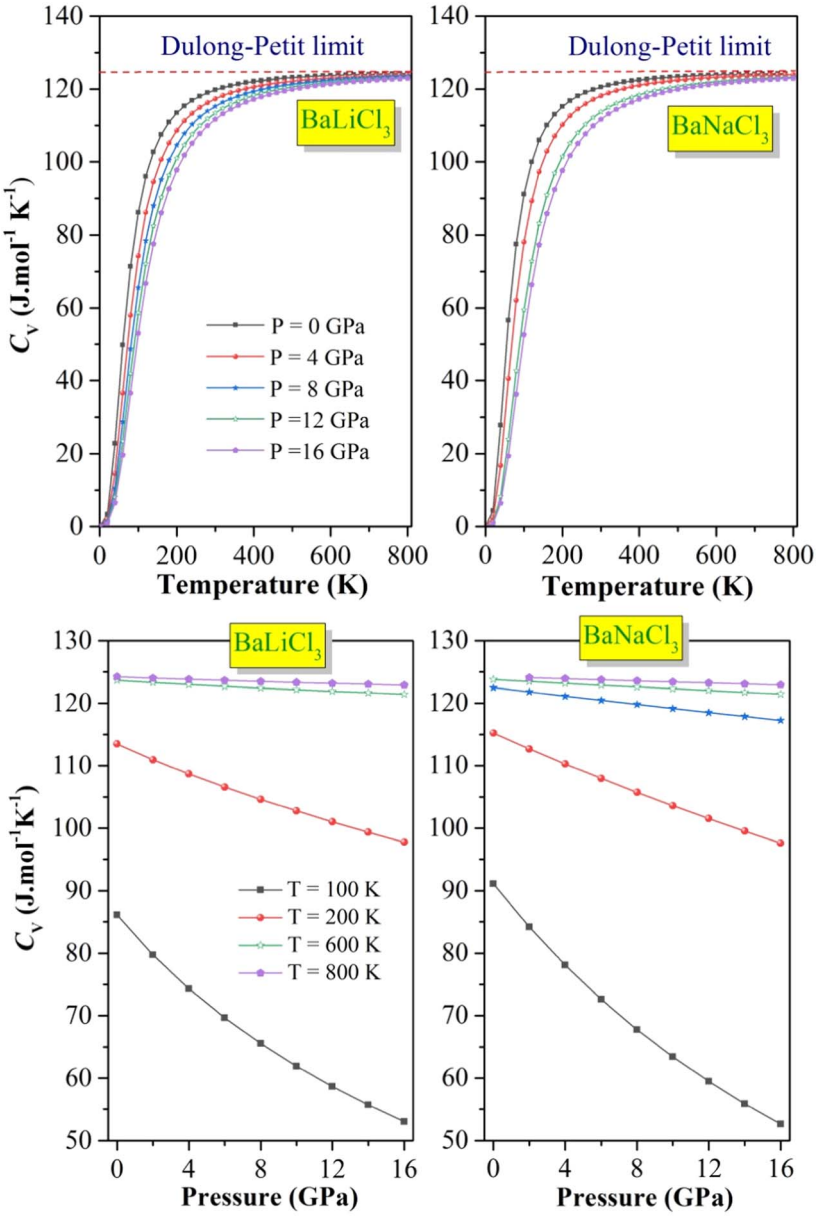

Figure 13. Evolutions of the of the isochoric heat capacities (C_V) with temperature at fixed pressures and with pressure at fixed temperatures for $BaLiCl_3$ and $BaNaCl_3$ perovskites.

failure. To quantify the degree of elastic anisotropy of crystals, some experimental and theoretical approaches have been developed. Visualization of the dependence of elastic moduli on crystal direction is the most used metric to characterize the elastic anisotropy of crystals. The three-dimensional (3D) representation of the dependence of an isotropic modulus of elasticity on crystal direction exhibits a perfect spherical shape. Therefore, the extent of the elastic anisotropy of a modulus of elasticity can be estimated from the deviation of its 3D representation from the perfect spherical shape. Crystal direction dependencies of the shear modulus (G) and Young's modulus (E) of a cubic system are expressed as follows [73, 74]:

$$G(\theta, \varphi) = (S_{44} + 4SJ)^{-1}$$

$$E(\theta, \varphi) = (S_{11} - 2SJ)^{-1}$$

$$S = S_{11} - S_{22} - 0.5S_{44}$$

$$J = sin^2\theta.cos^2\theta + 0.125sin^4\theta(1 - cos4\varphi)$$

Here S_{ij} are the elastic compliance constants, and θ and φ are the Euler angles. The 3D-representations of the Young's modulus and shear modulus as well as their 2D-representations in the $(xy)/(xz)/(yz)$ and $(x = y)$ planes for the title materials are illustrated in figures 8 and 9. The weak deviations of the 3D-representations and 2D-presentations of the Young's modulus (E) and shear modulus (G) of $BaLiCl_3$ crystal from the spherical and

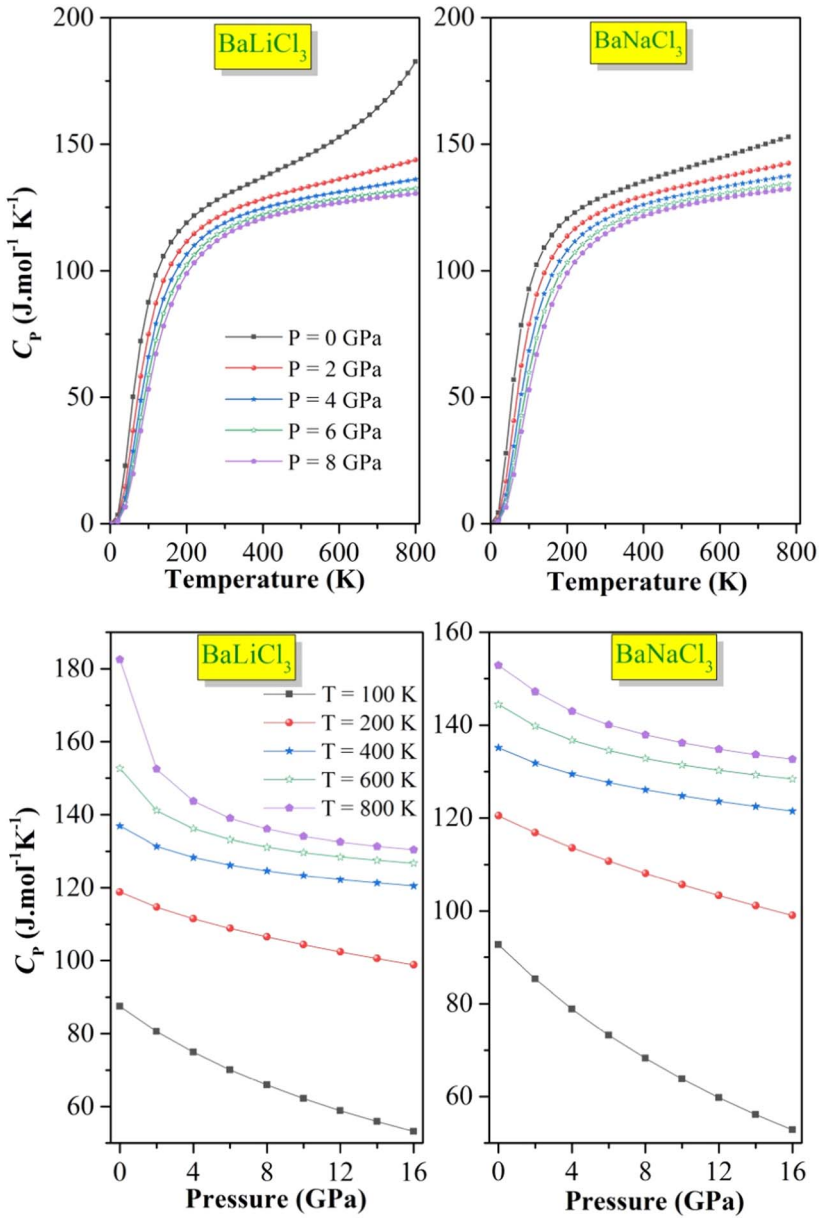

Figure 14. Evolutions of the of the isobar heat capacities (C_p) with temperature at fixed pressures and with pressure at fixed temperatures for $BaLiCl_3$ and $BaNaCl_3$ perovskites.

circular shapes, respectively, point out the weak elastic anisotropy of $BaLiCl_3$. However, the remarkable strong deviations of the 3D-representations and 2D-presentations of the Young's modulus and shear modulus (G) of $BaNaCl_3$ crystal from the spherical and circular shapes, respectively, highlight the strong elastic anisotropy of $BaNaCl_3$. The Young's modulus of $BaLiCl_3$ reaches its maximum (E_{max}) value of 62.7 GPa along the <100> crystal direction and its minimum (E_{min}) value of 55.5 GPa along the <111> direction. The maximum (G_{max}) and minimum (G_{min}) values of the shear modulus of $BaNaCl_3$, which occur along the <111> and <100> directions, respectively, are 24.3 and 22.5 GPa. The weak differences between the E_{max} and E_{min} and between G_{max} and G_{min} values confirm the weak elastic anisotropy of $BaLiCl_3$ crystal. For $BaNaCl_3$, the E_{max} value that occurs along the <100> direction, and the E_{min} value that occurs along the <111> direction, are equal to 73.0 and 23.6 GPa, respectively, and the G_{max} value that occurs along the <111> direction, and the G_{min} value that occurs along the <100> direction, are equal to 16.9 and 8.6 GPa, respectively. For $BaNaCl_3$, the E_{max} value is the triple of the E_{min} value and the G_{max} value is the double of the G_{min} value, highlighting the strong elastic anisotropy of the $BaNaCl_3$ crystal.

3.3. Thermodynamic properties

Materials are generally used in high temperature and pressure environment; it is therefore important to study their specific behavior when subjected to pressure and temperature effects. To examine the effects of pressure

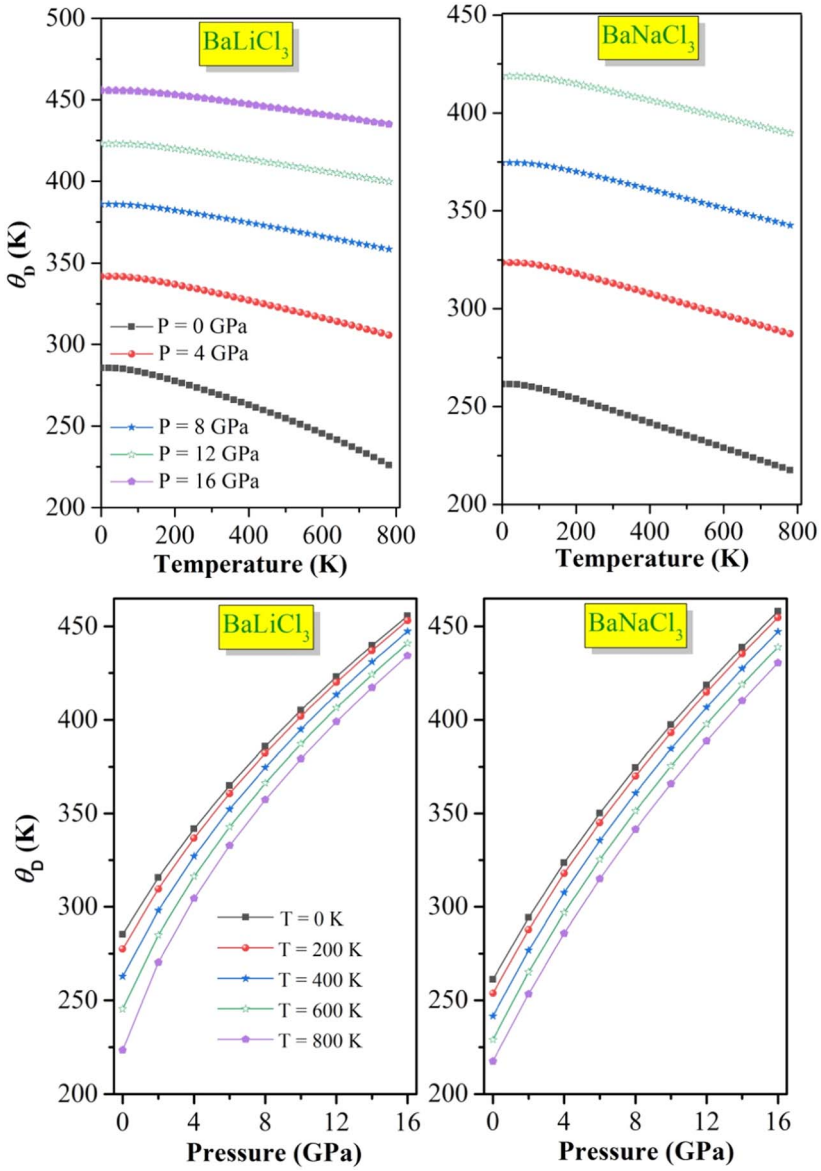

Figure 15. Evolutions of the Debye temperature (θ_D) with temperature at fixed pressures and with pressure at fixed temperatures for $BaLiCl_3$ and $BaNaCl_3$ perovskites.

and temperature on some macroscopic physical characteristic of the considered materials, the quasi-harmonic approximation as incorporated in the Gibbs computational software was used [39].

Evolutions of the lattice parameter (a) of $BaLiCl_3$ and $BaNaCl_3$ with temperature up to 800K at the fixed pressures: 0, 4, 8, 12, and 16 GPa, and with pressure up to 16 GPa at the fixed temperatures: 0, 200, 400, 600, and 800 are depicted in figure 10. It is well known that temperature and pressure have opposite effects on the lattice parameter a, which increases with increasing temperature at a fixed pressure and decreases with increasing pressure at a fixed temperature, as one can easily see it in figure 10.

Figure 11 shows the evolution of the modulus of compressibility (B) with temperature (T) and pressure (P) for $BaLiCl_3$ and $BaNaCl_3$. One notes B decreases with increasing T. Note that with increasing pressure, the decreasing rate of B with increasing T decreases. B is 32.5 GPa for $BaLiCl_3$ and 29.0 GPa for $BaNaCl_3$ at ambient temperature ($T = 300$K) and P zero pressure.

Figure 12 shows the changes in the volume thermal expansion coefficient (α) with temperature and pressure. It can be seen that with the increase in temperature, α increases rapidly up to 300K and then increases moderately. Note that the effect of temperature on α decreases remarkably with the increase of pressure, and it becomes small at high pressure. The thermal expansion coefficient is $12.01 \times 10^{-5}\,K^{-1}$ for $BaLiCl_3$ and $11.32 \times 10^{-5}\,K^{-1}$ for $BaNaCl_3$ at ambient temperature and zero pressure.

Figure 13 depicts the changes in isochoric heat capacity (C_V) with increasing temperature at fixed pressure and with increasing pressure at fixed temperature for of $BaXCl_3$ (X = Li, Na) compounds. For temperatures

below 300K, C_V increases rapidly with increasing temperature due to the exponential increase in the number of excitatory phonon modes in this temperature range. For temperatures above 300K, C_V increases slowly and tends at high temperature towards the well-known Dulong-Petit limit [75], which is approximately 124.6 $J.mol^{-1}.K^{-1}$. For temperatures above 500K, the effect of pressure on C_V is insignificant. As the pressure increases, C_V decreases. At Zero pressure and ambient temperature 300K, C_V is 119.79 $J.mol^{-1}.K^{-1}$ for $BaLiCl_3$ and 120.56 $J.mol^{-1}.K^{-1}$ for $BaNaCl_3$.

Figure 14 shows the changes in isobaric heat capacity (C_P) with temperature at fixed pressure and with pressure at fixed temperatures for $BaLiCl_3$ and $BaNaCl_3$. For temperatures lower than 300K, Cp increases rapidly with increasing temperature, then its decreasing rate becomes moderate. The increasing rate of Cp with temperature decreases with increasing pressure. At zero pressure and ambient temperature, C_P is approximately 129.50 $J.mol^{-1}.K^{-1}$ for $BaLiCl_3$ and $BaNaCl_3$.

Figure 15 shows the effects of temperature and pressure on the Debye temperature (θ_D) for $BaLiCl_3$ and $BaNaCl_3$. The Debye temperature decreases with increasing temperature at fixed pressures and increases with increasing pressure at fixed temperatures. This happens because as the pressure increases, the elastic wave velocities gradually increase as the binding forces strengthen and hence the Debye temperature increases [76]. As the Debye temperature is the highest temperature obtainable as a result of a single normal vibration, its increase and decrease with pressure and temperature, respectively, can be explained as follows. The increase of pressure, which causes the increase of the vibrational frequencies of anions and cations, will cause the increase of Debye temperature, while the increase of temperature that causes expansive distortions of the structure causes the increase of the wavelength of anions and cations vibrations, resulting in the decrease of the vibrational frequencies and, therefore, Debye temperature decreases. The calculated θ_D through the quasi-harmonic approximation at zero pressure and temperature is 285.4 K for $BaLiCl_3$ and 261.3 K for $BaNaCl_3$. Note that the calculated Debye temperature value from the elastic constants is in acceptable agreement with that calculated using the quasi-harmonic approximation.

4. Conclusion

This article presents the findings of a theoretical investigation into the structural, elastic, and thermodynamic properties of $BaXCl_3$ compounds (where X represents Li or Na) using the pseudopotential plane wave method based on the density functional theory. Various exchange-correlation functionals, including GGA-PBE, GGA-PBEsol, GGA-WC, and LDA, were utilized to calculate the structural properties. The GGA-PBEsol functional was chosen to compute the elastic and thermodynamic properties due to its ability to model exchange-correlation interactions for solids. The equilibrium lattice parameters obtained through these calculations matched well with previously reported results for the two compounds. The computed elastic constants demonstrated that $BaXCl_3$ (X = Li, Na) materials are mechanically stable even under hydrostatic pressures up to 18 GPa. Isotropic elastic moduli, such as the modulus of compressibility, Young's modulus, shear modulus, Poisson's ratio, speeds of sound, and Debye temperature, were calculated using well-known approximations from the elastic constant of monocrystalline materials. $BaNaCl_3$ exhibited strong elastic anisotropy, while $BaLiCl_3$ showed weak elastic anisotropy. Pugh's criterion suggested that $BaNaCl_3$ is ductile, whereas $BaLiCl_3$ can be classified as brittle under a pressure range of zero to 3.6 GPa, but exhibits ductile behavior at pressures greater than 3.6 GPa. Using the quasi-harmonic approximation, the effects of temperature and pressure on the lattice parameter, modulus of compressibility, isobaric and isochoric heat capacities, coefficient of volumetric thermal expansion, and Debye temperature were explored. These findings are theoretical predictions that require experimental verification in future studies, as no prior experimental or theoretical investigations exist on the properties under consideration.

Acknowledgments

The author S. Bin Omran acknowledges the Researchers Supporting Project number (RSP2023R82), King Saud University, Riyadh, Saudi Arabia.

Data availability statement

All data that support the findings of this study are included within the article (and any supplementary files).

Declaration of competing interest

There is on conflict of interest.

ORCID iDs

Missoum Radjai https://orcid.org/0000-0002-0313-7155
Saber Sâad Essaoud https://orcid.org/0000-0002-6337-3184

References

[1] Petrović M, Chellappan V and Ramakrishna S 2015 Perovskites: solar cells & engineering applications–materials and device developments *Sol. Energy* **122** 678–99
[2] Ayaz U, Shazia A, Husain M, Rahman N and Bonyah E 2021 Ab initio investigation of structural, electronic, magnetic, elastic, and optical properties of Cs-based chloro-perovskites $CsXCl_3$ (X = Be and Rh) *AIP Adv.* **11** 105215
[3] Reshak A H, Khan S, Laref A, Murtaza G and Bila J 2020 Pressure induced physical variations in the lead-free fluoropervoskites XYF_3 (X = K, Rb, Ag; Y = Zn, Sr, Mg): Optical materials *Opt. Mater.* **109** 110325
[4] Bayhan Ü and Yilmaz İ 2023 Prediction of structural, electronic, and lattice dynamical properties of ABO_3 [A = K, Rb, Cs; B = Sn, Sb] perovskite compounds *Physica* **649** 414355
[5] Hayatullah Murtaza G, Muhammad G, Naeem S, Khalid M N and Manzar A 2013 Physical properties of $CsSnM_3$ (M = Cl, Br, I): a first principle study *Acta Phys. Pol.* **124** 102–7
[6] Hamioud F and Mubarak A A 2018 Structural, elastic and optoelectronic properties of the hydrogen based perovskite compounds: *ab-initio* study *Chin. J. Phys.* **56** 1–9
[7] Ali M A, Wahab A, Murtaza G and Khan A 2019 First-principles calculations for structural, elastic, mechanical, electronic and optical properties of $CsYbCl_3$ *Mater. Res. Express* **6** 065905
[8] Nyayban A, Panda S and Chowdhury A 2023 The effect of B-site alloying on the electronic and opto-electronic properties of $RbPbI_3$: a DFT study *Physica B* **649** 414384
[9] Khandy S A and Gupta D C 2016 Structural, elastic and thermo-electronic properties of paramagnetic perovskite $PbTaO_3$ *RSC Adv.* **6** 48009–15
[10] Li J, Zhang X, Zhang Z, Liu T, Chen L and Liu Z 2023 Linear pseudo-halogen anion passivating defects for MAPbI3 perovskite solar cells *Physica* **651** 414591
[11] Mehmood M, Rasul M N, Hussain A, Rafiq M A, Iqbal F, Manzoor A and Khan M A 2023 Investigation of structural, electronic, elastic, magnetic and thermodynamic properties of antiperovskites $XCRh_3$ (X = Cd, Ta, W, Re, Os, Ir, Pt, Au, Hg, Ce, Pr, Nd, Pm, Sm, Eu, Tb) *Physica* **649** 414442
[12] Roknuzzaman M, Ostrikov K K, Wang H, Du A and Tesfamichael T 2017 Towards lead-free perovskite photovoltaics and optoelectronics by ab-initio simulations *Sci. Rep.* **7** 1–8
[13] Li L, Wang Y J, Liu D X, Ma C G, Brik M G, Suchocki A and Reshak A H 2017 Comparative first-principles calculations of the electronic, optical, elastic and thermodynamic properties of XCaF3 (X = K, Rb, Cs) cubic perovskites *Mater. Chem. Phys.* **188** 39–48
[14] Hayat S, Khalil R A, Hussain M I, Rana A M and Hussain F 2022 A DFT study of perovskite-type halides KBeBr3, RbBeBr3, and $CsBeBr_3$ in triclinic phase for advanced optoelectronic devices *Solid State Commun.* **344** 114674
[15] Qian Q, Wan Z, Takenaka H, Keum J K, Smart T J, Wang L and Duan X 2023 Photocarrier-induced persistent structural polarization in soft-lattice lead halide perovskites *Nat. Nanotechnol.* **18** 357–64
[16] Chen S and Shi G 2017 Two-dimensional materials for halide perovskite-based optoelectronic devices *Adv. Mater.* **29** 1605448
[17] Akman E, Shalan A E, Sadegh F and Akin S 2021 Moisture-resistant $FAPbI_3$ perovskite solar cell with 22.25% power conversion efficiency through pentafluorobenzyl phosphonic acid passivation *ChemSusChem* **14** 1176–83
[18] Tailor N K, Listorti A, Colella S and Satapathi S 2023 Lead-free halide double perovskites: fundamentals, challenges, and photovoltaics applications *Adv. Mater. Technol.* **8** 2200442
[19] Adinolfi V, Peng W, Walters G, Bakr O M and Sargent E H 2018 The electrical and optical properties of organometal halide perovskites relevant to optoelectronic performance *Adv. Mater.* **30** 1700764
[20] Mubarak A A 2014 The elastic, electronic and optical properties of $RbCaX_3$ (X = F, Cl) compounds *Int. J. Mod. Phys.* **28** 1450192
[21] Naeem S, Murtaza G, Khenata R and Khalid M N 2013 First principle study of $CsSrM_3$ (M = F, Cl) *Physica B* **414** 91–6
[22] Murtaza G, Khenata R, Muhammad S, Reshak A H, Wong K M, Omran S B and Alahmed Z A 2014 Structural, chemical bonding, electronic and magnetic properties of KMF_3 (M = Mn, Fe, Co, Ni) compounds *Comput. Mater. Sci.* **85** 402–8
[23] Mubarak A A and Al-Omari S 2015 First-principles calculations of two cubic fluoropervskite compounds: $RbFeF_3$ and $RbNiF_3$ *J. Magn. Magn. Mater.* **382** 211–8
[24] Yalameha S, Saeidi P, Nourbakhsh Z, Vaez A and Ramazani A 2020 Insight into the topological phase and elastic properties of halide perovskites $CsSnX_3$ (X = l, Br, Cl) under hydrostatic pressures *J. Appl. Phys.* **127** 085102
[25] Yang J H, Yin W J, Park J S and Wei S H 2016 Fast self-diffusion of ions in CH 3 NH 3 PbI 3: the interstitialy mechanism versus vacancy-assisted mechanism *J. Mater. Chem. A* **4** 13105–12
[26] Xiao Z, Du K Z, Meng W, Mitzi D B and Yan Y 2017 Chemical origin of the stability difference between copper (I)-and silver (I)-Based halide double perovskites *Angew. Chem.* **129** 12275–9
[27] Zhao X G, Yang J H, Fu Y, Yang D, Xu Q, Yu L and Zhang L 2017 Design of lead-free inorganic halide perovskites for solar cells via cation-transmutation *J. Am. Chem. Soc.* **139** 2630–8
[28] Xiao Z, Meng W, Wang J, Mitzi D B and Yan Y 2017 Searching for promising new perovskite-based photovoltaic absorbers: the importance of electronic dimensionality *Materials Horizons* **4** 206–16
[29] Gómez-Peralta J I and Bokhimi X 2021 Ternary halide perovskites for possible optoelectronic applications revealed by Artificial Intelligence and DFT calculations *Mater. Chem. Phys.* **267** 124710
[30] Segall M D, Lindan P J, Probert M A, Pickard C J, Hasnip P J, Clark S J and Payne M C 2002 First-principles simulation: ideas, illustrations, and the CASTEP code *J. Phys. Condens. Matter* **14** 2717

[31] Clark S J, Segall M D, Pickard C J, Hasnip P J, Probert M I, Refson K and Payne M C 2005 First principles methods using CASTEP *Zeitschrift für kristallographie-crystalline materials* **220** 567–70
[32] Perdew J P, Ruzsinszky A, Csonka G I, Vydrov O A, Scuseria G E, Constantin L A and Burke K 2008 Restoring the density-gradient expansion for exchange in solids and surfaces *Phys. Rev. Lett.* **100** 136406
[33] Perdew J P, Burke K and Ernzerhof M 1996 Generalized gradient approximation made simple *Phys. Rev. Lett.* **77** 3865
[34] Haas P, Tran F and Blaha P 2009 Calculation of the lattice constant of solids with semilocal functionals *Phys. Rev.* **79** 085104
[35] Hedin L and Lundqvist B I 1971 Explicit local exchange-correlation potentials *J. Phys.* **4** 2064
[36] Vanderbilt D 1990 Soft self-consistent pseudopotentials in a generalized eigenvalue formalism *Phys. Rev.* **41** 7892
[37] Monkhorst H J and Pack J D 1976 Special points for Brillouin-zone integrations *Phy. Rew.* **13** 5188
[38] Fischer T H and Almlof J 1992 General methods for geometry and wave function optimization *J. Phys. Chem.* **96** 9768–74
[39] Blanco M A, Francisco E and Luana V 2004 GIBBS: isothermal-isobaric thermodynamics of solids from energy curves using a quasi-harmonic Debye model *Comput. Phys. Commun.* **158** 57–72
[40] Birch F 1947 The finite elastic strain of cubic crystals *Phys. Rev.* **71** 809
[41] Birch F 1978 Finite strain isotherm and velocities for single-crystal and polycrystalline NaCl at high pressures and 300 K *Journal of Geophysical Research: Solid Earth* **83** 1257–68
[42] Vinet P J J R, Ferrante J, Smith J R and Rose J H 1986 A universal equation of state for solids *J. Phys.* **19** L467
[43] Li C, Lu X, Ding W, Feng L, Gao Y and Guo Z 2008 Formability of abx3 (x = f, cl, br, i) halide perovskites *Acta Crystallogr., Sect. B: Struct. Sci* **64** 702–7
[44] Khan A, Ullah U A, Tirth I, Algahtani V, A and Zaman A 2022 DFT study of the structural, elastic and optoelectronic properties of Cu-based cubic halide-perovskites $ACuF_3$ (A = Mg and Ca) *Phys. Scr.* **97** 085819
[45] Khuili M *et al* 2023 First-principles study of structural, elastic, optoelectronic and thermoelectric properties of B-site-ordered quadruple perovskite $Ba_4Bi_3NaO_{12}$ *J. Solid State Chem.* **322** 123955
[46] Suetin D V and Shein I R 2018 Electronic structure, mechanical and dynamical stability of hexagonal subcarbides M 2 C (M = Tc, Ru, Rh, Pd, Re, Os, Ir, and Pt): *Ab Initio* Calculations *Phys. Solid State* **60** 213–24
[47] Gherriche A, Bouhemadou A, Al-Douri Y, Bin-Omran S, Khenata R and Hadi M A 2021 *Ab initio* exploration of the structural, elastic, electronic and optical properties of a new layered perovskite-type oxyfluoride: $CsSrNb_2O_6F$ *Mater. Sci. Semicond. Process.* **131** 105890
[48] Yoo C Y, Hong K P and Kim S J 2007 A new layered perovskite, KSrNb2O6F, by powder neutron diffraction *Acta Crystallogr., Sect. C: Cryst. Struct. Commun.* **63** i63–5
[49] Choy J-H, Kim J-Y, Kim S-J, Sohn J-S and Han O H 2001 New dion– Jacobson-type layered perovskite oxyfluorides, $ASrNb_2O_6F$ (A = Li, Na, and Rb) *Chem. Mater.* **13** 906–12
[50] Radjai M, Bouhemadou A and Maouche D 2021 Structural, elastic, electronic, and optical properties of the half-Heusler ScPtSb and YPtSb compounds under pressure arXiv:2112. 09940
[51] Reshak A H and Jamal M 2012 DFT calculation for elastic constants of orthorhombic structure within WIEN2K code: a new package (ortho-elastic) *J. Alloys Compd.* **543** 147–51
[52] Grimvall G 1999 *Thermophysical Properties of Materials* (Amsterdam: Elsevier)
[53] Karki B B, Clark S J, Warren M C, Hsueh H C, Ackland G J and Crain J 1997 *Ab initio* elasticity and lattice dynamics of *J. Phys. Condens. Matter* **9** 375
[54] Liu Q J, Ran Z, Liu F S and Liu Z T 2015 Phase transitions and mechanical stability of TiO2 polymorphs under high pressure *J. Alloys Compd.* **631** 192–201
[55] Hill R 1952 The elastic behaviour of a crystalline aggregate *Proc. of the Physical Society. Section A* 65, 349
[56] Voigt W 1910 *Lehrbuch der kristallphysik:(mit ausschluss der kristalloptik* (Leipzig: BG Teubner) 34
[57] Reuss A J Z A M M 1929 Calculation of the flow limits of mixed crystals based on the plasticity of monocrystals *Z. Angew. Math. Mech* **9** 49–58
[58] Karim A M M T, Jubair M, Nuruzzaman M and Zilani M A K 2022 An ab initio study on the mechanical stability, spin-dependent electronic properties, molecular orbital predictions, and optical features of antiperovskite A_3InN (A = Co, Ni) *ACS Omega* **7** 13588–603
[59] Bouhemadou A 2008 Calculated structural and elastic properties of M_2InC (M = Sc, Ti, V, Zr, Nb, Hf, Ta) *Modern Physics Letters* **22** 2063–76
[60] Pugh S F 1954 XCII. relations between the elastic moduli and the plastic properties of polycrystalline pure metals *The London, Edinburgh, and Dublin Philosophical Magazine and Journal of Science* **45** 823–43
[61] Mattesini M, Magnuson M, Tasnadi F, Höglund C, Abrikosov I A and Hultman L 2009 Elastic properties and electrostructural correlations in ternary scandium-based cubic inverse perovskites: a first-principles study *Physical Review B* **79** 125122
[62] Radjai M, Guechi N and Maouche D 2021 An *ab initio* study of structural, elastic and electronic properties of hexagonal MAuGe (M = Lu, Sc) compounds arXiv:2103.15579
[63] Rahman M A, Hasan W, Khatun R, Hasan M Z, Rahman M H, Sarker S and Lubna J F 2023 An ab-initio study to investigate the structural, mechanical, electrical, optical and thermal properties of the AZrO3 (A = Mg, Ca, Sr, Ba, Sn, Cu) compounds *Mater. Today Commun.* **34** 105339
[64] Radjai M, Bouhemadou A and Bin-Omran S 2022 Ab initio study of pressure dependence of the structural, elastic and thermodynamic properties of $AlXY_3$ (X = B, C) *Phase Transit.* **96** 1–15
[65] Wachter P, Filzmoser M and Rebizant J 2001 Electronic and elastic properties of the light actinide tellurides *Physica B* **293** 199–223
[66] Sun Z, Li S, Ahuja R and Schneider J M 2004 Calculated elastic properties of M_2AlC (M = Ti, V, Cr, Nb, and Ta) *Solid State Commun.* **129** 589–92
[67] Anderson O L 1963 A simplified method for calculating the Debye temperature from elastic constants *J. Phys. Chem. Solids* **24** 909–17
[68] Kanchana V, Vaitheeswaran G, Svane A and Delin A 2006 First-principles study of elastic properties of CeO_2, ThO_2, and PoO_2 *J. Phys. Condens. Matter* **18** 9615
[69] Jasiukiewicz C and Karpus V 2003 Debye temperature of cubic crystals *Solid State Commun.* **128** 167–9
[70] Miah M K, Hossain K M, Rahman M A, Rasheduzzaman M, Mitro S K, Modak J K and Hasan M Z 2021 Comprehensive study on the physical properties of tetragonal La T Ge3 (T = Rh, Ir, or Pd) compounds: an ab initio investigation *AIP Adv.* **11** 025046
[71] Sarker S, Rahman M A and Khatun R 2021 Study of structural, elastic, electronics, optical and thermodynamic properties of Hf2PbC under pressure by ab-initio method *Comput. Condens. Matter* **26** e00512
[72] Khireddine A, Bouhemadou A, Alnujaim S, Guechi N, Bin-Omran S, Al-Douri Y and Kushwaha A K 2021 First-principles predictions of the structural, electronic, optical and elastic properties of the zintl-phases AE_3GaAs_3 (AE = Sr, Ba). *Solid State Sci.* **114** 106563
[73] Nye J F 1985 *Physical Properties of Crystals: Their Representation by Tensors and Matrices* (Oxford: Oxford University Press)

[74] Luan X, Qin H, Liu F, Dai Z, Yi Y and Li Q 2018 The mechanical properties and elastic anisotropies of cubic Ni3Al from first principles calculations *Crystals* **8** 307
[75] Petit A T and Dulong P L 1819 Research on some important aspects of the theory of heat *Ann. Philos.* **14** 189–98
[76] Liu Z J, Tan X M, Guo Y, Zheng X P and Wu W Z 2009 Thermodynamic properties of $CaSiO_3$ perovskite at high pressure and high temperature *Z. Naturforsch.* **64** 399–404